Thermodynamic analyses of different scenarios in a CCHP system with micro turbine – Absorption chiller, and heat exchanger

Mojtaba Mirzaee[a], Reza Zare[b], Milad Sadeghzadeh[c], Heydar Maddah[a], Mohammad Hossein Ahmadi[d], Emin Acıkkalp[e], Lingen Chen[f,*]

[a] *Energy Institute of Higher Education, Saveh 39177-67746, Iran*
[b] *Department of Chemical Engineering, Shahreza Branch, Islamic Azad University, Shahreza, Iran*
[c] *Department of Renewable Energy and Environmental Engineering, University of Tehran, Tehran, Iran*
[d] *Faculty of Mechanical Engineering, Shahrood University of Technology, Shahrood, Iran*
[e] *Department of Mechanical and Manufacturing Engineering, Engineering Faculty, Bilecik Seyh Edebali University, Bilecik, Turkey*
[f] *Institute of Thermal Science and Power Engineering, Wuhan Institute of Technology, Wuhan 430205, China*

ARTICLE INFO	ABSTRACT
	Distributed generation as a viable solution to the energy crisis has gained popularity in recent years due to reduced transmission losses and improved efficiency. In this study, nine scenarios are considered to analyze and evaluate a cogeneration system in various conditions. The cogeneration system that includes a gas turbine, absorption chillers, boilers, and heat exchangers is modeled in EES software. The system is studied in multiple scenarios. Values of energy efficiency (EE), used energy (UE), and utility fuel ratio (UFR) are calculated to assess the system. In addition, the amount of CO_2 production is also investigated for each of the scenarios. It is found that the system used in scenario No. 5 which consists of two absorption chillers installed in series, with UFR of 45325.50 kJ/kg has the optimum performance in terms of simultaneous electricity and cooling generation. For electricity and heating generation, scenario No. 7 in which heat can be completely recovered, with UFR of 39541.90 kJ/kg is the optimum configuration. It is monitored that scenario No. 1 and scenario No. 6 have the highest amount of carbon dioxide production among the studied scenarios, 88.18 kg/s.

1. Introduction

Fossil fuels which are the prime energy resources have been depleting severely in recent years. As can be seen in Fig. 1, fossil fuels form over 81% of the total energy use [1]. These resources emit large amounts of carbon dioxide and noxious gases leading to climate change and air pollution [2,3]. Moreover, economic concerns, energy crisis, and environmental footprints pose obstacles to the energy sector [4]. Therefore, new policies should be developed to optimize energy performance as well as meeting energy demand.

The total efficiency of thermal power plants ranges from 30 to 50% [5,6]. Electricity should also be transmitted over long distances that showed up to 20% loss. Distributed generation, defined as energy production close to the consumer, can mitigate the transmission losses [7–9]. CHP systems take advantage of the waste heat of an engine that produces electricity. CCHP or tri-generation is an integration of CHP and absorption or compression chillers that can produce heating, cooling, and power simultaneously. The energy efficiency of these

systems can reach to 60–90% as well as showing a 35% better performance than conventional plants in microgeneration [10–12]. CCHP systems can also decrease the amount of carbon dioxide emission [13,14]. The efficiency of CCHP systems is 50% higher than CHP systems. Moreover, the systems enjoy advantages in terms of energy-saving, job creation, safety, etc. [15,16]. However, the major restriction toward vast application of distributed energy production systems such as CHP or CCHP is their disability to meet the peak demand in some specific periods [17].

In recent years, there has been an increasing amount of literature on distributed generation. By way of illustration, Pagliarini et al. [18] analyzed the feasibility of a tri-generation layout for a hospital in Parma, Italy. They found that the primary energy saving index is insufficient for optimizing engine size of the tri-generation system. Moreover, the economic analysis showed that the maximum annual money-saving occurs when the electrical capacity coincides with the mid-load, i.e., the load between the peak and the base. Jabbari et al. [19] designed and optimized a CCHP system for the paper industry.

Nomenclature

$C_{p,mix}$	Specific heat capacity of flue gas (kJ/kg.K)
$h'_{C,in}$	Enthalpy at the inlet of the compressor (kJ/kg)
$h'_{C,out}$	Enthalpy at the outlet of the compressor (kJ/kg)
$h'_{T,in}$	Enthalpy value at the inlet of the turbine (kJ/kg)
$h'_{T,out}$	Enthalpy value at the outlet of the turbine (kJ/kg)
k	Specific heat ratio
LHV	Lower heating value (kJ/kg)
$\dot{m}_{air}$	Mass flow rate of the air (kg/s)
$\dot{m}_{T,in}$	Inlet mass flow rate of the turbine (kg/s)
$\dot{Q}_{cooling}$	Required rate of cooling load (kW)
$\dot{Q}_g$	Required rate of heat (kW)
$\dot{Q}_{heating}$	Actual rate of heating load (kW)
r_p	Pressure ratio
$T_{C,in}$	Temperature at the inlet of the compressor
$T_{C,out}$	Temperature at the outlet of the compressor
$T_{1,g}$	Input temperature of flue gas in the boiler
$T_{2,g}$	Output temperature of flue gas in the boiler
$\dot{W}_C$	Required power for the compressor (kW)

$\dot{W}_T$	Power output of the turbine (kW)

Greek symbols

η_b	Efficiency of the boiler
η_C	Compressor efficiency
η_T	Turbine efficiency

Abbreviations

CCHP	Combined cooling, heating and power
CHP	Combined heating and power
COP	Coefficient of performance
DEAC	Double effect absorption chiller
EE	Energy efficiency
MT	Micro turbine
NG	Natural gas
SEAC	Single effect absorption chiller
UE	Used energy
UFR	Utility fuel ratio (kJ/kg)

Their system consisted of a CHP cycle and an absorption heat pump. They employed Aspen Plus software for simulating the process. They also used a genetic algorithm to optimize the system. They considered two objective functions and five decision parameters to optimize the CHP cycle. They performed the optimization on the absorption heat pump by considering six parameters associated with the geometry of heat exchangers, pressure drop and a single objective function to reduce total annual costs. Their economic analyses revealed that with a reasonable payback period, the proposed system could be cost-efficient. Zhou et al. [20] examined the design and operation of a CCHP system while neglecting the dynamic characteristics of the equipment. Their equipment can be easily moved from one operating point to another, enabling the system to meet the fluctuating energy need. To provide electricity, cooling, and domestic hot water need, Wang et al. [21] simulated a CCHP system under different circumstances. They indicated that their proposed CCHP system had a better performance than the previous systems with higher investment costs. Al-Qattan et al. [22] studied a solid oxide fuel cell and gas turbine in a CCHP application integrated to absorption chillers and a thermal storage tank. Their study indicated that fuel consumption and carbon emissions were reduced by 54%. Jayasekara and Halgamuge [23] simulated a novel cycle for absorption chiller and compared it with a double effect absorption chiller. The main advantage of their method over the previous single and

double effect chillers is the wider range of temperature with a relatively increased coefficient of performance (COP). The proposed chiller can be added to their system as a slightly modified single or double effect chiller. Ebrahimi and Keshavarz [24] designed a hybrid CCHP system for a residential building considering five climatic conditions. They also optimized a solar collector in terms of size, type, and orientation. To determine the size of the prime mover, they applied the maximum rectangle method. They specified solar annual heat gain for each climate. They showed that bigger engine sizes could reduce the size of collectors, and the smaller engines could increase the fuel energy saving. They also found that when basic CCHP operates were in full load, more fuel could be saved; by contrast, hybrid CCHP used less fuel when it operates in partial load. Hanafizadeh et al. [25] designed a CCHP for a workplace and commercial construction that consist of a series of blocks in Tehran, Iran. In this regard, they evaluated hourly energy demand throughout the year and considered three plausible scenarios to determine the size of the prime mover according to electricity production capacity. In the first scenario, electricity production was higher than the demand, in the second scenario electricity was produced on the basis of peak load, and in the last scenario, the load was estimated based on the primary load of the building. They selected eight alternatives according to the engine, the capacity of turbines and indicators of each scenario. They compared the alternatives by considering economic aspects. As a result, they selected a 4×4 MW wind turbine as the adequate type in terms of the optimum values of NPV (net present value), IRR (internal rate of return) and NP (normal payback). To select an effective refrigeration system considering different distances for steam transport, Li and Hu [26] performed an exergy analysis. Exergy and energy efficiency analyses of the system demonstrated that the steam transport distance and extraction steam pressure should be lower than 5 km and 0.65 MPa, respectively. With careful selection of input steam pressure, they commented that the exergy efficiency of the absorption refrigeration system could be equal to or higher than the electric compression refrigeration system. Gang et al. [27] examined the performance of a refrigeration system combined with different energy systems in subtropical regions. They concluded that the ice storage system was not a viable alternative in Hong Kong due to the current feed-in tariff. Moreover, their study demonstrated that production of the cooling load by the district cooling system integrated with CCHP system was more profitable than providing electricity from the grid. Wang et al. [28] examined the effect of a dual-source absorption chiller used in a CCHP system which can operate using solar heat and waste heat of an internal combustion engine. Their
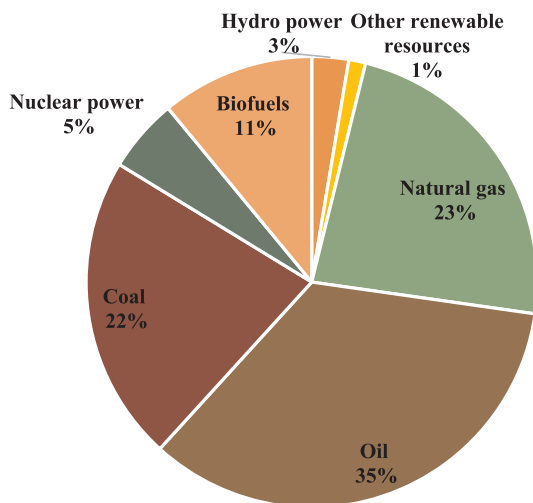

Fig. 1. Global energy share of different resources in 2015 [1].

findings showed that the system operation while working with solar heat was determined by solar radiation. To improve the efficiency of an organic Rankin cycle (ORC) using a CCHP system, Chaiyat et al. [29] reduced condenser temperature of an absorption system. Their integrated system showed a better performance when the condenser temperature was decreased. Their ORC performance can be increased by 7% when the condenser temperature was 15°C. Their economic assessment demonstrated that electricity costs produced by the modified system were greater than the normal system. Goyal et al. [30] studied performance and greenhouse gas emissions of a small scale CCHP system that operates based on a single-cylinder diesel engine. Their findings suggested that CO_2 emissions per kWh were declined in CCHP, CHP and CCP (combined cooling and power) systems by 57.46, 53.83 and 8.02%, respectively, compared with conventional types. Wang et al. [31] analyzed a CCHP which was driven by an internal combustion engine fired by natural gas and biomass gasification gas. Their findings indicated that the proposed system could improve primary energy saving. Wang et al. [32] proposed a new CCHP and presented an inclusive thermodynamic assessment. Han et al. [33] presented a multi-generation system of cooling, heating, and power with a solution energy storage medium without any heat preservation system. Caliano et al. [34] recommend a strategy for biomass-fired CCHP systems to meet the time-varying energy demands of an Italian residential section. Wang et al. [35] presented a CCHP layout including a gas turbine, an absorption chiller, a storage medium, and a solar parabolic trough collector which was used as the air-preheater before entering into the turbine. The authors performed thermodynamic-economic-environmental analysis on the presented system and reported that the system exergy efficiency was 24.9% in the cooling mode and 25.7% in the heating status. In addition, the integration of solar collector was beneficial in decreasing the amount of carbon emission up to 41%. Mehrpooya et al. [36] analyzed the feasibility of utilizing a CCHP unit based on solid oxide fuel cell (SOFC) for residential applications. The proposed structure showed the total efficiency (including cooling, heating, and electricity generation modes) of 60%. Sheykhi et al. [37] carried out an investigation to find out the effect of applying a Stirling engine to a conventional internal combustion engine based CHP system. Results showed that the Stirling engine brought about several beneficial

impacts in the fields of thermal efficiency and economic considerations. Wu et al. [38] investigated the application of introducing solar thermal systems in the CCHP systems from economic aspects. Abbasi et al. [39] performed a techno-economic analysis on a CCHP unit with gas engine, diesel engine, and gas turbine as the major driving system in various configurations. it was found from the results that the combination mode of two driving unit was performing better that the single driving system. Adhami et al. [40] studied a CCHP system consists of a micro-gas turbine and a micro-absorption chiller. The overall weight of the system was about 14 kg which is practical in several applications. Wang et al. [41] combined a gas-turbine driven CCHP with solar and compressed air storage unit. The overall exergy efficiency of the proposed system was reported to be 53.1%.

Chen and his colleges [42–52] performed energy, exergy, and exergoeconomic analyses and optimizations of various gas turbine-based CHP [42–46] and CCHP [48,49,51] plants, including simple, regenerative, inter-cooling, and regenerated gas turbine-based cogeneration system plants by using thermodynamic optimization theory [53–77].

The purpose of this paper is to enhance the overall thermal efficiency of combined systems. Thus, a multi-generation system that includes a micro-turbine (driving unit), absorption chillers (conventional H_2O-LiBr as the working fluids), boilers, and heat exchangers will be introduced and modeled in the EES software. Two models of single-effect and double-effect absorption chillers were considered and applied in the tri-generation system. The system will be studied in multiple defined-scenarios to take advantage of the waste heat of flue gas discharging from the turbine. In this study, nine scenarios will be considered to evaluate the performance of the multi-production design in various conditions. Then, the system will be compared to determine the most practical scenario in different cases including cooling and power, heating and power, and combined cooling, heating, and power .

2. System description

A conventional co-generation comprises a prime mover, heat recovery system and systems that generate heating and cooling load by using the recovered heat. The configuration of cogeneration systems
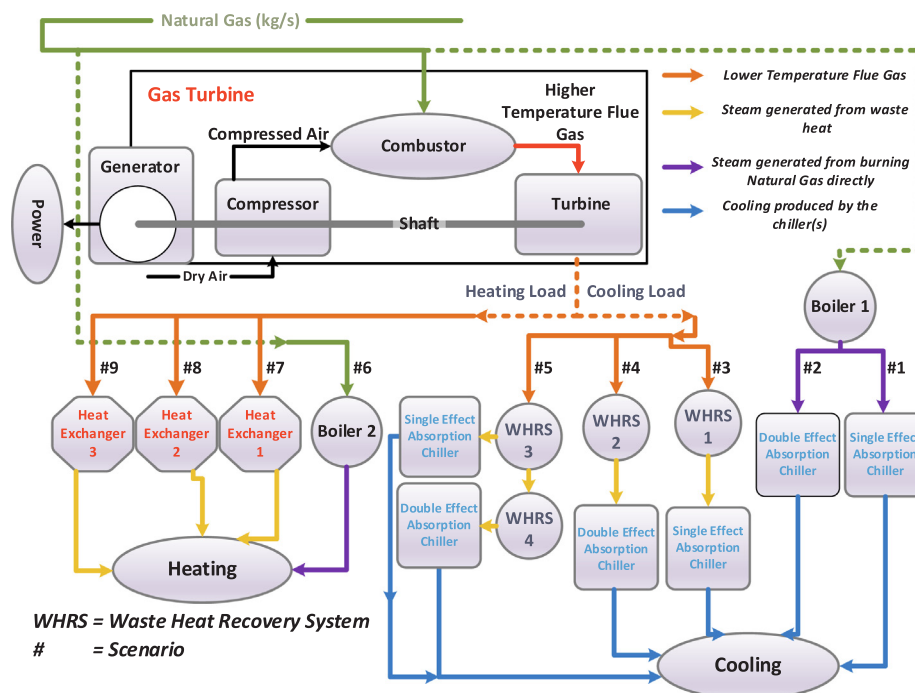

Fig. 2. Schematic of the system under study.

depends on the cycle applied to the system, required heat and power, and heat recovery techniques. Fig. 2 shows a schematic of the system presented in this study. In this study, a microturbine (MT) is implemented (a compressor, a combustion chamber, and a turbine). Initially, dry air enters the compressor. After compression, the air enters the combustion chamber where natural gas (NG) and dry air are combusted. The hot flue gas coming out of the combustion chamber runs the expansion turbine to convert the kinetic energy into the mechanical energy. A generator is also used to produce electrical power from mechanical energy. The high-temperature exhaust gas from the turbine can be utilized to produce heating and cooling loads. In cooling, the high-temperature exhaust gas enters into the waste heat recovery system (WHRS) to provide energy for absorption chillers. To produce the heating load, the gas is used in the heat exchanger (Hex) to produce steam. If the exhaust gas is not recoverable, a separate boiler running on NG is used to produce hot water and steam. Therefore, boiler no. 1 is implemented to meet the energy need of single and double effect chillers (SEAC, DEAC) and boiler no. 2 is utilized to produce steam for heating.

In this research, it is assumed that the required electricity is provided by a MT in all seasons. During the summer, in addition to the electricity, the refrigeration is carried out by an absorption chiller. Here, two types of absorption chillers are studied·H_2O-LiBr are the utilized working fluids in the absorption chillers.

In the first scenario, electricity is generated by the use of natural gas by the MT, and the single-effect absorption chiller consumes natural gas separately and provides the required cooling load.

The 2nd scenario is similar to scenario (1) whilst a double-effect absorption chiller is employed. In scenario (3), the exhaust gas from the MT enters into the heat exchanger and the produced steam is consumed by a single-effect absorption chiller, so NG consumption is reduced. The scenario (4) is similar to scenario (3), but the type of used chiller is replaced with a double-effect chiller. In the heat recovery section of the 5th scenario both single-effect and double-effect absorption chiller are utilized, which improves the energy recovery performance.

In the winter, electricity is supplied by the MT, and the required heat is supplied by a boiler or a heat exchanger. In scenario (6), consumption of NG in both units of micro-turbine and boiler providing the demanded load of electricity and heat. In scenario (7), the exhaust gas from the MT enters into the heat exchanger, and the resulted hot water is used for heating. Therefore, the consumption of NG is decreased in the 7th scenario. Scenarios (8) and (9) are similar to scenario (7), but the amount of recovered heat is different in each scenario.

3. Microturbine modeling

All of the MTs operate based on the Brayton cycle. The number of stages and configuration of the system can vary from one turbine to another. However, all the turbine cycles follow the sequence of compression, combustion, and expansion.

3.1. Compressor modeling

Pressurization of working fluid is one of the prime processes of Brayton cycle that can be done by a compressor [78,79]. Having passed through the expansion turbine, the pressure of working fluid drops. Therefore, the compressor should provide the required pressure for the fluid to circulate through the cycle [80]. The schematic process of the compressor is depicted in Fig. 3.

To compress the air, the compressor requires mechanical energy. The energy can be provided by a shaft connected to the expansion turbine. The efficiency of compressor plays a significant role in the total efficiency of MT since 55–60% of the generated power is internally consumed in the power cycle by the compressor [81]. The required power for the compressor is given by [82]:

$$\dot{W}_C = \dot{m}_{air}(h_{C,out} - h_{C,in}) \tag{1}$$

where $\dot{m}_{air}$ is the mass flow rate of the air, $h_{C,out}$ is the enthalpy at the outlet and $h_{C,in}$ is the enthalpy at the inlet of the compressor.

When the air is compressed, the temperature increases with the pressure. Considering that the compression process is adiabatic, the actual enthalpy at the compressor outlet can be assessed from the following equation [82]:

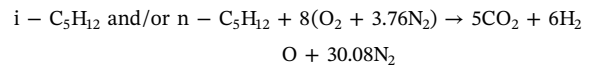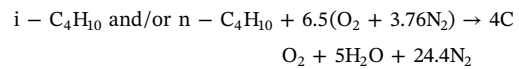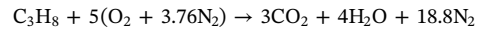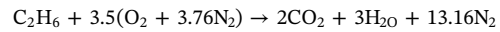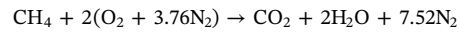$$h_{C,out} = \frac{h'_{C,out} - h_{C,in}}{\eta_C} + h_{C,in} \tag{2}$$

where η_C is the compressor efficiency and $h'_{C,out}$ is the output enthalpy of the ideal (isentropic) compressor. Employing the ideal gas assumption, the temperature at the outlet of the compressor can be evaluated by [82]:

$$T_{C,out} = \frac{T_{C,in}[r_p^{\frac{k-1}{k}} - 1]}{\eta_C} + T_{C,in} \tag{3}$$

r_p denotes the pressure ration and k is the specific heat ratio.

3.2. Combustion chamber modeling

Fig. 4 indicates inputs and output of the combustion chamber. Fuel consumed in the combustion process is NG with a fixed composition. The fuel reacts with oxygen in dry air consisting of O_2 and N_2 in an isobaric process. The combustion equations are presented below [82]:

$CH_4 + 2(O_2 + 3.76N_2) \rightarrow CO_2 + 2H_2O + 7.52N_2$

$C_2H_6 + 3.5(O_2 + 3.76N_2) \rightarrow 2CO_2 + 3H_2O + 13.16N_2$

$C_3H_8 + 5(O_2 + 3.76N_2) \rightarrow 3CO_2 + 4H_2O + 18.8N_2$

$i - C_4H_{10}$ and/or $n - C_4H_{10} + 6.5(O_2 + 3.76N_2) \rightarrow 4C$
$\qquad\qquad O_2 + 5H_2O + 24.4N_2$

$i - C_5H_{12}$ and/or $n - C_5H_{12} + 8(O_2 + 3.76N_2) \rightarrow 5CO_2 + 6H_2$
$\qquad\qquad O + 30.08N_2$

Input mass flow rate to the turbine can be expressed as:

$$\dot{m}_{T,in} = \dot{m}_{air} + NG \tag{4}$$

where NG is the mass flow rate of the fuel.

The process of combustion is assumed to be stoichiometric, complete and adiabatic [83,84]. Therefore, the efficiency of the combustion process is considered as 100%.

The input enthalpy of the turbine can be obtained using the following equation [82]:

$$h_{T,in} = \frac{\dot{m}_{air}h_{C,out} + (NG \times LHV)}{\dot{m}_{T,in}} \tag{5}$$

where LHV is the lower heating value. Specific heat of gas exhausted from the combustion chamber can be calculated by [82]:

$$C_{p,mix} = \sum x_i C_{p,i} \tag{6}$$

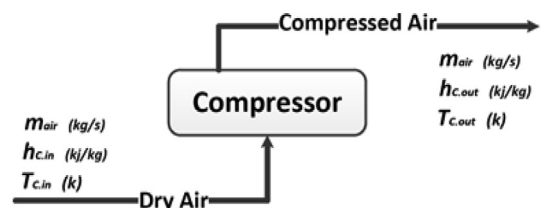where x_i is the molar fraction of gases.

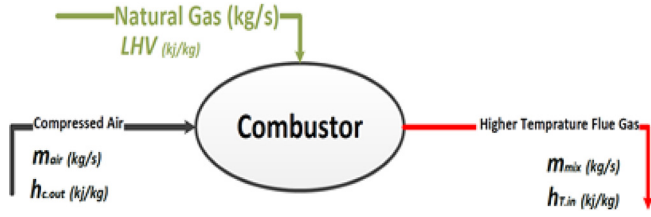**Fig. 3.** The working fluid flow in the compressor.
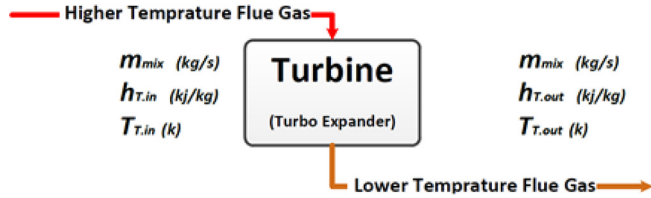
Fig. 4. Fuel and airflow to the combustion chamber.

Fig. 5. The flow of flue gas in the expansion turbine.

Table 1
Scenarios description.

Scenario No	Demand	Description
1	Power &Cooling	MT&SEAC are active and work separately
2	Power &Cooling	MT&DEAC are active and work separately
3	Power &Cooling	MT&SEAC are active and integrated
4	Power &Cooling	MT&DEAC are active and integrated
5	Power &Cooling	MT& SEAC &DEAC are active and integrated
6	Power &Heat	MT&Boiler are active and work separately
7	Power &Heat	MT&HRSG are integrated (T_2.g = 408.150 K)
8	Power &Heat	MT&HRSG are integrated (T_2.g = 443.150 K)
9	Power &Heat	MT&HRSG are integrated (T_2.g = 473.150 K)

3.3. Expansion turbine modeling

Fig. 5 shows the flow of flue gas in an expansion turbine. The expansion of hot and compressed flue gas in the turbine is considered to adiabatic. The power output of the turbine is [82]:

$$\dot{W}_T = \dot{m}_{T,in}(h_{T,in} - h_{T,out}) \tag{7}$$

where $\dot{m}_{T,in}$ is the inlet mass flow rate of the turbine, $h_{T,in}$ and $h_{T,out}$ are enthalpy values at the inlet and outlet of the turbine, respectively.

Enthalpy of air at the outlet of the turbine is given by [82]:

$$h_{T,out} = h_{T,in} - \eta_T(h_{T,in} - h'_{T,out}) \tag{8}$$

where η_T is isentropic efficiency of the turbine and $h'_{T,out}$ is the enthalpy at the outlet of the isentropic turbine. Consequently, employing the ideal gas behavior, the temperature at the outlet of the turbine is [82]:

$$T_{T,out} = T_{T,in} - \eta_T T_{T,in}\left(1 - \frac{1}{r_P^{\frac{k-1}{k}}}\right) \tag{9}$$

4. Scenario descriptions

A simple Brayton cycle is applied to meet electricity demand. Moreover, to meet the heating and cooling loads, boilers, heat exchangers and absorption chillers are utilized in the system. Accordingly, nine scenarios are considered. In the first five scenarios, the system is designed to fulfill electricity and cooling need. These scenarios are based on the assumption that the minimum required cooling load is 100 ton equivalent to 351.7 kW of refrigeration. The next four scenarios are considered to provide electricity and heating load. The following is a detailed account of the scenarios under consideration.

4.1. Scenario No. 1

In the first scenario, a single effect absorption chiller (SEAC) is utilized to provide cooling. In this case, the waste heat of flue gas of MT cannot be recovered. Hence, MT is used to generate power.

Absorption chillers require heat to separate refrigerant from absorber in the generator. The required rate of heat $\dot{Q}_g$ is calculated based on the coefficient of performance (COP) [82]:

$$\dot{Q}_g = \dot{Q}_{cooling}/COP \tag{10}$$

where, $\dot{Q}_{cooling}$ is the required rate of cooling load.

A boiler is also considered in this scenario to produce hot water or steam required for the chiller. The amount of NG consumed in the boiler is [82]:

Table 3
NG analysis injected into the combustion chamber.

Component	Mole Percent	Molecular Weight	LHV (kJ/kg)
N_2	0.14	28.00	48,594
CO_2	0.41	46.00	
CH_4	84.70	16.04	
C_2H_6	9.97	30.07	
C_3H_8	3.62	44.09	
i-C_4H_{10}	0.36	58.12	
n-C_4H_{10}	0.65	58.12	
i-C_5H_{12}	0.08	72.15	
n-C_5H_{12}	0.07	72.15	
Total	100	–	

Table 4
Combusted NG analysis.

Component	O_2 Required	H_2O Produced	N_2 Produced	CO_2 Produced
N_2	–	–	0.14	–
CO_2	–	–	–	0.64
CH_4	169.40	169.40	636.94	84.70
C_2H_6	34.89	29.91	131.20	19.94
C_3H_8	18.10	14.48	68.05	10.86
i-C_4H_{10}	2.34	1.80	8.79	1.44
n-C_4H_{10}	4.22	3.25	15.88	2.60
i-C_5H_{12}	0.64	0.48	2.41	0.40
n-C_5H_{12}	0.56	0.42	2.10	0.35
Total	230.15	219.74	865.51	120.70

Table 5
Analysis of flue gas with and without excess air.

Component	Mole Percent (%)		C_{Pi} (kJ/kg.K)
	With excess air	Without excess air	
N_2	72	76.01	1.042
CO_2	10	4.13	0.842
H_2O	18	7.52	1.872
O_2	–	12.34	0.922

Table 2
Properties of the input and output air to the compressor.

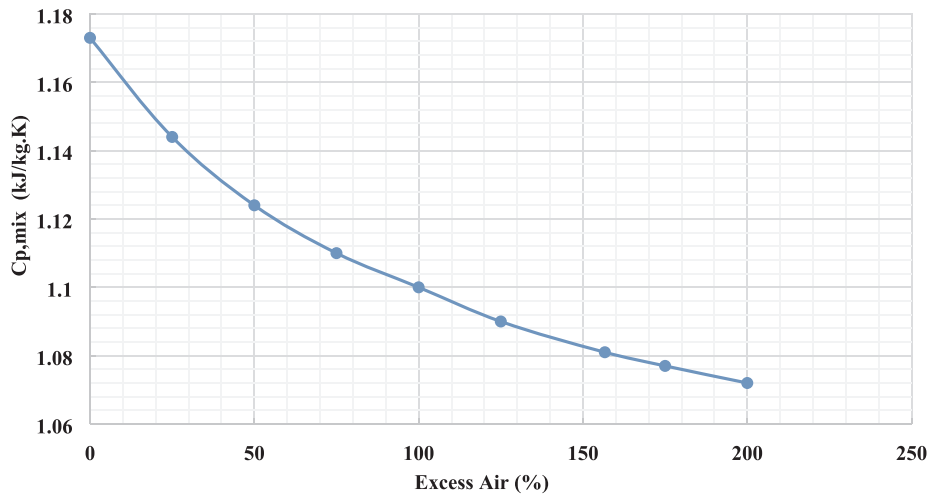| Compressor	$P_{C.in}$ (atm)	$P_{C.out}$ (atm)	$T_{C.in}$ (k)	$T_{C.out}$ (k)	$h_{C.in}$ (kJ/kg)	$h_{C.out}$ (kJ/kg)	$h'_{C.out}$	k	C_P (kJ/kg.k)
1	11	298.150	651.810	299.343	654.413	601.153	1.410	1.004

Fig. 6. Variations of $C_{p,mix}$ to excess air.

Table 6
MT performance.

MT	NG (kg/s)	$\dot{W}_{net}(kW)$	UE (kW)	Utility (kW)	EE (%)	UFR (kJ/kg)
	0.019	311.683	311.683	311.683	34	16536.660

Table 7
Performance of SEAC and boiler for scenario No. 1.

SEAC		Boiler 1		
$\dot{Q}_{cooling}(kW)$	COP	$\dot{Q}_g(kW)$	η_b	NG (kg/s)
351.700	0.730	481.781	0.850	0.012

$$NG = \frac{\dot{Q}_g}{LHV \times \eta_b} \tag{11}$$

where η_b is the boiler efficiency.

4.2. Scenario No. 2

Similar to the previous scenario, MT produces power. Nevertheless, to produce cooling load, a double-effect absorption chiller (DEAC) is employed. DEAC enjoys an advantage in terms of *COP*. Eqs. (10) and (11) can be employed to obtain the required heating load and amount of *NG* consuming in the system.

4.3. Scenario No. 3

In this scenario, not only the gas turbine provides mechanical energy for electricity generation, but also it produces the heating load required for SEAC. The chiller recovers the waste heat of flue gas discharged from the MT using WHRS No. 1, to provide its required energy. MT is fed with natural gas. Since the waste heat is recovered, no boiler is used in this scenario. Therefore, the amount of NG consumed in the system is equal to the amount of NG fed to MT. Value of $\dot{Q}_g$ obtained in the first scenario should also be generated in this scenario to provide

Table 9
Performance of DEAC and boiler for scenario No. 2.

DEAC		Boiler 1		
$\dot{Q}_{cooling}(kW)$	COP	$\dot{Q}_g(kW)$	η_b	NG (kg/s)
351.700	1.200	293.083	0.850	0.007

the desired cooling load. The mass flow rate of flue gas is calculated by [82]:

$$\dot{Q}_g = Mass\ flow\ rate\ of\ flue\ gas \times C_{p,mix}(T_{1,g} - T_{2g}) \tag{12}$$

$$Mass\ flow\ rate\ of\ flue\ gas = \frac{\dot{Q}_g}{C_{p,mix}(T_{1,g} - T_{2,g})} \tag{13}$$

where $C_{p,mix}$ is the specific heat capacity of flue gas, and $T_{1,g}$ and $T_{2,g}$ are the input and output temperatures of flue gas in the boiler, respectively.

4.4. Scenario No. 4

A DEAC is employed in this case and there is no need for the boiler to provide the heating load. The required amount of heat for DEAC is obtained from WHRS No. 2 which is fed with flue gas of MT. However, due to constraints on temperature and pressure in this type of chiller, the recovery system cannot completely recover the heat of flue gas, which results in heat loss. Considering that the mass flow rate of flue gas to produce 351.7 kWh cooling load has been calculated in the previous scenario, Eq. (12) is used to calculate the amount of recoverable heat. Moreover, using *COP* of the chiller and Eq. (10) the cooling load is obtained. The amount of NG equals to that consumed in MT.

4.5. Scenario No. 5

In this scenario, it is strived to fully exploit the heat of flue gas. Two absorption chillers are utilized in series. After rotating the blades of the turbine, the flue gas runs into the heat recovery system (WHRS 3)

Table 8
Performance of the system in scenario No. 1.

System	NG (kg/s)	$\dot{W}_{net}(kW)$	$\dot{Q}_g(kW)$	$\dot{Q}_{cooling}(kW)$	UE (kW)	Utility (kW)	EE (%)	UFR (kJ/kg)
MT	0.019	311.683	–	–	311.683	311.683	34	21741.700
SEAC	0.012	–	481.781	351.700	481.781	351.700	–	

Table 10
Performance of the system in scenario No. 2.

System	NG (kg/s)	$\dot{W}_{net}(kW)$	$\dot{Q}_g(kW)$	$\dot{Q}_{cooling}(kW)$	UE (kW)	Utility (kW)	EE (%)	UFR (kJ/kg)
MT	0.019	311.683	–	–	311.683	311.683	34	25570.190
DEAC	0.007	–	293.083	351.700	293.083	351.700	–	

Table 11
Performance of SEAC and WHRS in scenario No. 3.

SEAC			WHRS 1			
Q_Cooling (kW)	COP	$\dot{Q}_g(kW)$	$C_{p.mix}$ (kj/kg.k)	$T_{1.g}$ (K)	$T_{2.g}$ (K)	Mass flow rate Flue Gas (kg/s)
351.700	0.730	481.781	1.081	949.942	408.150	0.822

Table 13
Performance of WHRS in scenario No. 4.

WHRS 2				
Flue Gas (kg/s) (kg/s)	$C_{p.mix}$ (kJ/kg.K)	$T_{1.g}$ (K)	$T_{2.g}$ (K)	$\dot{Q}_g(kW)$
0.822	1.081	949.942	493.150	406.196

connected to DEAC to provide the heating load considering constraints on temperature. Then, the gas passes through the recovery system (WHRS 4) connected to SEAC. After interaction with the recovery system, the gas temperature drops to over dew point temperature. Finally, the gas is exhausted to the atmosphere.

Eq. (12) is employed to assess the amount of heat generated in the two recovery systems. Input temperature of the flue gas to WHRS 3 is equal to the output temperature of WHRS 4. According to the recovered heat in the recovery systems and *COP* of the chillers, the cooling load is calculated by applying Eq.(10). The cooling load in this scenario is the sum of cooling loads of both chillers. The amount of NG is equivalent to that consumed in MT.

4.6. Scenario No. 6

Heating load is required in this scenario. Therefore, absorption chillers are omitted and only a boiler (boiler No. 2) is considered to produce steam. Similar to scenarios Nos. 1 and 2, waste heat of the flue gas is irrecoverable. In addition to MT, NG should be also added to the boiler. The amount of fuel added to MT and the boiler forms the total amount of fuel consumption in the system. The boiler burns NG to produce steam for heating applications. However, due to heat losses, the rate of actual heat $\dot{Q}_{heating}$ is not equal to the rate of extracted heat $\dot{Q}_g$. The actual rate of the heating load is [82]:

$$\dot{Q}_{heating} = 0.9\dot{Q}_g \tag{14}$$

4.7. Scenario No. 7

In this scenario, the heat of the exhaust gas of MT is completely recoverable. Thus, a heat exchanger is substituted to generate steam (and the boiler is removed). NG is only consumed in the MT. Moreover, values of $\dot{Q}_g$ and $\dot{Q}_{heating}$ are calculated by using Eqs. (12) and (14), respectively.

4.8. Scenario No. 8

On the condition that running costs of heat exchangers to fully recover the heat of exhaust gas are not affordable, scenarios Nos. 8 and 9 are defined. Moreover, the scenarios can compare the performance of CHP systems. In scenario No. 8, it is assumed that the efficiency of the heat exchanger is lower than the efficiency of the exchanger used in the

previous scenario. The exchanger can turn about 93% of the recovered heat into steam in scenario No. 8. According to the output temperature of the heat exchanger used in this scenario, values of $\dot{Q}_g$ and $\dot{Q}_{heating}$ are calculated (Eqs. (12) and (14)).

4.9. Scenario No. 9

The efficiency of the heat exchanger for scenario No. 9 is approximately 88%. And Eqs. (12) and (14) are used to assess the values of $\dot{Q}_g$ and $\dot{Q}_{heating}$.

All of the 9 scenarios summarization are listed in Table 1.

5. Energy efficiency

The amount of fuel consumption differs from one scenario to another. The efficiency of the boiler is defined separately. Moreover, the COP which is used to express the performance of the chillers relies on efficiency. Thus, the total efficiency of the system is equivalent to the amount of useful energy of the fuel in the gas turbine and is expressed as follows [82]:

$$EE = \frac{(\dot{W}_{net} + \sum \dot{Q}_g)}{LHV \times NG} \tag{15}$$

6. Used energy, utility and utility fuel ratio

In order to compare the energy generated and the fuel efficiency in each scenario, the total energy efficiency of the system is not sufficient. Hence, used energy, utility, and utility fuel ratio parameters will be defined to gain a better understanding of the performance of the scenarios.

6.1. Used energy

Used energy parameter is the total energy extracted from the fuel for each scenario and can be obtained from the following equation:

$$UE = \dot{W}_{net} + \sum \dot{Q}_g \tag{16}$$

6.2. Utility

Based on consumer energy need, i.e., heating, cooling, and

Table 12
Performance of the system in scenario No. 3.

System	NG (kg/s)	$\dot{W}_{net}$ (kW)	$\dot{Q}_g$ (kW)	$\dot{Q}_{cooling}$ (kW)	UE (kW)	Utility (kW)	EE (%)	UFR (kJ/kg)
MT + SEAC	0.019	311.683	481.781	351.700	793.464	663.383	86.60	35196.470

Table 14
Performance of the system in scenario No. 4.

System	NG (kg/s)	$\dot{W}_{net}$ (kW)	$\dot{Q}_g$ (kW)	$\dot{Q}_{cooling}$ (kW)	UE (kW)	Utility (kW)	EE (%)	UFR (kJ/kg)
MT + DEAC	0.019	311.683	406.196	487.435	717.879	799.118	78.40	42398.020

Table 15
Performance of the chillers and boilers in scenario 5.

	Part of Boilers					Part of Chillers	
	Flue Gas (kg/s)	$C_{p.mix}$ (kJ/kg.K)	$T_{1.g}$ (K)	$T_{2.g}$ (K)	$\dot{Q}_g (kW)$	COP	$\dot{Q}_{cooling}(kW)$
DEAC	0.822	1.081	949.942	493.150	406.196	1.2	487.435
SEAC			493.150	408.150	75.585	0.730	55.177

electricity, the final energy generated in each scenario termed as utility parameter is assessed using the following equation:

$$Utility = \dot{W}_{net} + \dot{Q}_{heating} + \dot{Q}_{cooling} \tag{17}$$

6.3. Utility fuel ratio

The utility fuel ratio parameter (UFR) specifies the amount of energy that can be extracted from the unit mass of fuel. The UFR is obtained by dividing the utility parameter with the fuel consumption in each scenario:

$$UFR = \frac{\sum Utility}{\sum Mass\ flow\ rate\ of\ Natural\ gas} \tag{18}$$

7. Results and discussions

The cogeneration system is initially modeled in the EES software. The results obtained from the scenarios and MT modeling are discussed in the following sections.

7.1. Results obtained for gas turbine

Properties of the input air to the compressor and output air from the compressor are listed in Table 2. Value of specific enthalpy is obtained from specific heat ratio and pressure ratio. The pressure ratio of the turbine with axial compressor ranges from 5 to 15 with an optimal value of 11.

Considering that the isentropic efficiency of the compressor is 85%, the actual output value of enthalpy is calculated. The actual temperature of the flue gas in the compressor outlet is also obtained.

According to the fuel consumption in the combustion chamber, the mass flow rate of the air input to the compressor is calculated. Results of NG analysis injected into the chamber is summarized in Table 3.

Based on Table 3, the molecular mass of NG is found to be 19.1 kg/kmol. In this study, the required amount of NG for electricity generation is taken to be 0.01885 kg/s. The required air for complete combustion is assessed at 0.3131 kg/s on the basis of the mass flow rate of NG and stoichiometric relations. Therefore, the mass flow rate of the gas discharged from the combustion chamber equals the sum of flow rates of NG and the required air for combustion. After combustion, the flue gas

consists of N_2, O_2, and CO_2. Amounts of the compositions are listed in Table 4.

The ideal enthalpy of gas exhausted from the combustion chamber is assessed at 1701.115 kJ/kg by applying Eq. (5). To calculate the ideal input temperature at the turbine, the enthalpy should be divided by the specific heat of the flue gas. The flue gas specific heat $C_{p,mix}$ is 1.17 kJ/kg.K which is obtained using Eq. (6) and Table 5. Consequently, the ideal input temperature introducing to the turbine is 2835.34 K which is a high temperature.

The high temperature may lead to deformation of the turbine owing to operation in high tension. In real conditions, the optimum input temperature (allowable maximum temperature) is 1623.15 K. This parameter is given by the turbine manufacturer and for this study is assumed to be 1623.15 K (1350 °C). Since input temperature at the turbine (2835.34 K) is greater than allowable maximum temperature, excess air should be added to the compressor to lower the actual temperature. The exact amount of the excess air to reach the optimum input temperature (allowable maximum temperature) at the turbine, is estimated through trial and error. The output temperature of the combustion chamber and the flue gas composition correlate with the excess air. $C_{p,mix}$ also changes with variation of the flue gas composition. Fig. 6 demonstrates variations of $C_{p,mix}$ to the excess air.

Injection of 156.66 percent excess air to the MT can optimize input temperature (1621.275 K) introducing to the turbine. Findings of flue gas analysis for this case are also presented in Table 5. Having specified the exact amount of input air to the MT i.e. required air for combustion and the excess air, mass flow rate of the flue gas is obtained. The actual output enthalpy of the combustion chamber is calculated by using the mass flow rate and actual output enthalpy of the compressor. Temperature of the flue gas in turbine inlet is 1621.275 K which will not disrupt the performance of the system since the maximum allowable temperature is 1623.15 K. The actual output enthalpy is assessed at 1027.213 kJ/kg and the actual output temperature is 949.942 K. Performance of the MT is summarized in Table 6.

7.2. Results of scenarios

Heat and power produced by the MT are studied in multiple scenarios. In the following sections, the results of the study for the scenarios are discussed.

7.2.1. Scenario No. 1

It is assumed that the flue gas discharged from the turbine cannot be recovered, therefore a SEAC with a COP of 0.73 is included in the system. The maximum energy required for SEAC is 351.7 kW of cooling. The efficiency of the boiler is 0.85. So that amount of fuel required for the boiler is calculated using Eq. (14). Performance of the boiler and SEAC is listed in Table 7.

The total amount of fuel in this scenario is the sum of fuel used in MT and boiler1 (for SEAC support). The fuel is used to generate power in the MT and energy in the boiler. Therefore, UE is the sum of Q_g and $\dot{W}_{net}$. Value of utility for the MT and SEAC is equal to $\dot{W}_{net}$ and $\dot{Q}_{cooling}$,
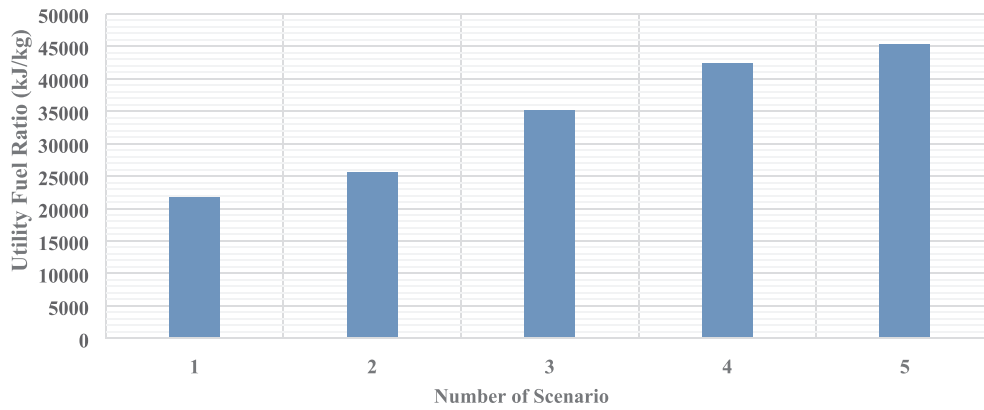
Table 16
Performance of the system in scenario No. 5.

System	NG (kg/s)	$\dot{W}_{net}$ (kW)	$\dot{Q}_g$ (kW)	$\dot{Q}_{cooling}$ (kW)	UE (kW)	Utility (kW)	EE (%)	UFR (kJ/kg)
MT + SEAC + DEAC	0.019	311.683	481.781	542.612	793.464	799.118	86.60	42398.02

Fig. 7. Values of UFR for scenarios Nos. 1–5.

Table 17
The system's performance based on the scenario No. 6.

System	NG (kg/s)	$\dot{W}_{net}(kW)$	$\dot{Q}_g(kW)$	$\dot{Q}_{heating}(kW)$	UE (kW)	Utility (kW)	EE (%)	UFR (kJ/kg)
MT	0.019	311.683	–	–	311.683	311.683	34	24425.980
Boiler 6	0.012	–	481.781	433.602	481.781	433.602	–	

Table 18
Performance of Hex in scenario No. 7.

HEx 1				
Flue Gas (kg/s)	$C_{p.mix}$ (kJ/kg.K)	$T_{1.g}$ (K)	$T_{2.g}$ (K)	$\dot{Q}_g(kW)$
0.822	1.081	949.942	408.150	481.781

Table 19
Performance of Hex in scenario No. 8.

	Flue Gas (kg/s)	$C_{p.mix}$ (kJ/kg.K)	$T_{1.g}$ (K)	$T_{2.g}$ (K)	$\dot{Q}_g(kW)$
HEx2	0.822	1.081	949.942	443.150	450.658

Table 21
Performance of HEx in scenario No. 9.

	Flue Gas (kg/s)	$C_{p.mix}$ (kJ/kg.K)	$T_{1.g}$ (K)	$T_{2.g}$ (K)	$\dot{Q}_g(kW)$
HEx3	0.822	1.081	949.942	473.150	423.981

7.2.3. Scenario No. 3

The energy required to generate 351.7 kW of cooling is determined by *COP* of the chiller. In this scenario, the flue gas temperature in WHRS inlet is equal to the output gas temperature of MT. Output temperature of WHRS ($T_{2, g}$) is 408.15 K. It should be noted that if $T_{2,g}$ decreases to less than 408.15, corrosion occurs. Based on the data, the flow rate of the flue gas is specified. Performance of WHRS and SEAC is listed in Table 11.

Fuel is only consumed in the turbine to provide the required power and cooling loads. Moreover, no fuel is required for the boiler which leads to the higher efficiency of the system. Performance of the system is listed in Table 12.

7.2.4. Scenario No. 4

The flue gas of the MT is utilized to meet the energy need of DEAC. The flow rate of the flue gas is similar to the previous scenario. In DEAC, steam with a pressure of 8 atm is required for the generator. The 8 atm steam has a temperature of 443 K. For steam generation in this pressure, the temperature of flue gas discharged from WHRS cannot be reduced to below 443 K. In real conditions, the efficiency of the boiler is lower than 100%. Therefore, the output temperature of WHRS is not equal to the steam temperature. The output temperature of WHRS is 493.15 K. Performance of WHRS is listed in Table 13.

Due to constraints on temperature which are mentioned earlier, the value of Q_g is reduced, leads to lower efficiency. However, cooling load increases owing to the high performance of DEAC. Consequently, values of utility and UFR increase that show a better performance than the

respectively. To determine UFR, $\dot{W}_{net}$ produced by MT and $\dot{Q}_{cooling}$ produced by SEAC should be divided by the total fuel. The fuel is only consumed to produce power. Thus, the value of EE is obtained from dividing $\dot{W}_{net}$ by specific heat of NG. Performance of the system for scenario No. 1 is listed in Table 8.

7.2.2. Scenario No. 2

The chiller and MT considered in this scenario is a DEAC with a COP of 1.2. Since COP of DEAC is higher than COP of SEAC, the energy required to produce 351.7 kW cooling decreases. As a result, the amount of fuel consumption in the system is reduced. Table 9 lists the performance of the boiler 1 (for DEAC support) and DEAC.

Reduction of fuel in cooling production improves the overall efficiency of the system. Considering the amount of fuel used for cooling and the fuel consumption in the turbine for power generation, the overall performance of the system can be assessed. Table 10 lists the overall performance of the system for the second scenario.

Table 20
Performance of the system in scenario No. 8.

System	NG (kg/s)	$\dot{W}_{net}$ (kW)	$\dot{Q}_g$ (kW)	$\dot{Q}_{heating}$ (kW)	UE (kW)	Utility (kW)	EE (%)	UFR (kJ/kg)
MT + HEx2	0.019	311.683	450.658	405.592	762.341	745.286	83.20	38055.750

Table 22
Performance of the system in scenario No. 9.

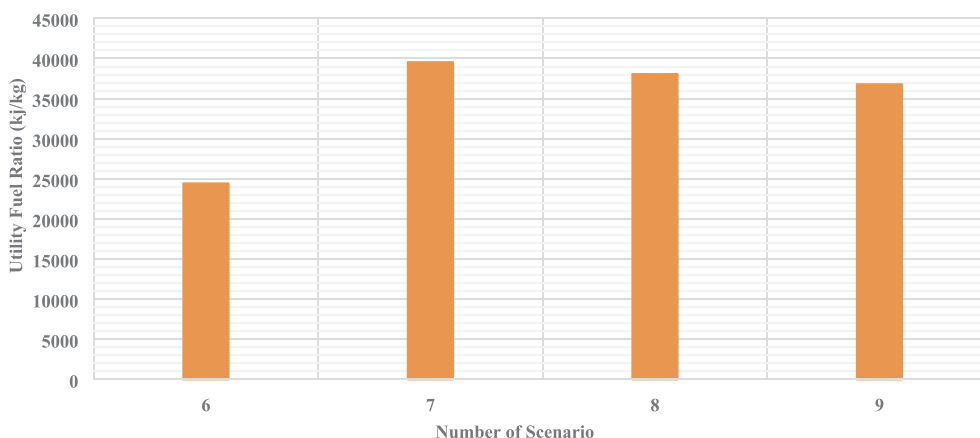| System	NG (kg/s)	$\dot{W}_{net}$ (kW)	$\dot{Q}_g$ (kW)	$\dot{Q}_{heating}$ (kW)	UE (kW)	Utility (kW)	EE (%)	UFR (kJ/kg)
MT + HEx3	0.019	311.683	423.981	381.582	735.663	693.266	80.30	36781.910

Fig. 8. Values of UFR for scenarios No. 6–9.
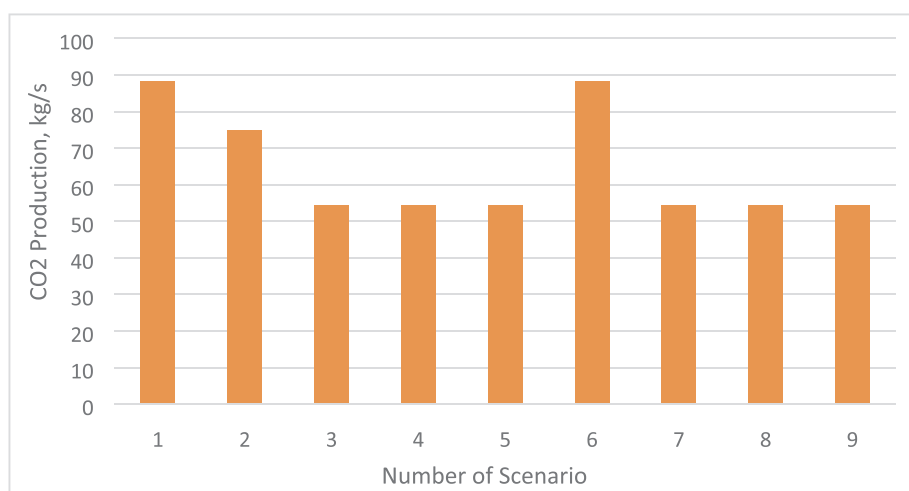
Fig. 9. Amount of CO_2 production in different scenarios.

previous scenarios. System performance is summarized in Table 14.

7.2.5. Scenario No. 5

Considering that 493.15 K is a high temperature for the flue gas, the energy of the flue gas can be exploited to provide energy need of SEAC and DEAC chillers installed in series. Therefore, useful heat of the gas can be fully exploited. The discharged temperature of the flue gas decreases to 408.15 K. Table 15 lists the performance of the chillers and their boilers.

Efficiency of the system is enhanced since the useful heat of the flue gas is totally recovered. Fuel which is injected to the system provides energy for MT, SEAC, and DEAC, and also leads to higher values of UE, Utility, and UFR. System performance is listed in Table 16.

Fig. 7 compares the utility fuel ratio of the first five scenarios. As can be seen, the performance of the system is more acceptable when electricity and cooling are generated simultaneously.

7.2.6. Scenario No. 6

A boiler running on NG is considered in this scenario for heating. The amount of NG consumed in boiler 6 is equal to that of boiler 1 in the first scenario. Consequently, $\dot{Q}_g$ is also equal to the corresponding value in scenario No. 1. Energy loss of the generated steam for heating purposes is taken to be 10%. The total amount of fuel in this scenario is the sum of fuel consumed in MT and boiler. Thus, a large amount of fuel is consumed in this scenario which results in poor performance of the system. Table 17 lists the system's performance for this scenario.

7.2.7. Scenario No. 7

No boiler is required if the capacity of the flue gas is totally used for heat production. In this scenario, flue gas at the temperature of 949.942 K enters into the heat exchanger (HEx 1). Considering that HEx is designed to use the total capacity of the flue gas, output temperature of the gas decreases to dew point temperature which is 408.15 K. According to the flow rate of the gas which is similar to the previous scenario, the amount of recovered heat can be obtained. Table 18 lists the performance of HEx 1.

90% of the produced steam is used for heating applications and 10% is lost. Since less fuel is consumed in this scenario, the performance of the system is improved.

7.2.8. Scenario No. 8

In this scenario, flue gas is discharged into the atmosphere at the temperature of 443.15 K. Less heat can be recovered while the output temperature of HEx is increasing. The amount of recovered energy and output temperature are listed in Table 19.

Fuel injected to the MT is of equal amount in all the studied scenarios. With decreasing heat recovery, fuel efficiency is also declining. Thus, the system shows poor performance in scenario No. 8. Performance of the system is listed in Table 20.

7.2.9. Scenario No. 9

The temperature of the flue gas emitted to the atmosphere is 473.15 K. Similar to the previous scenario the system performance is unfavorable. Performances of Hex and system are listed in Tables 21 and 22, respectively.

Performance of the last four scenarios is compared based on UFR in Fig. 8. As can be seen, the most efficient scenario in terms of fuel consumption is scenario No. 7. It is noteworthy that these scenarios are set to meet electricity and heating demand.

The amount of carbon dioxide production in each scenario is depicted in Fig. 9. As it is monitored from Fig. 9, scenarios 1 and 6 due to their higher amount of fuel consumption generate a larger amount of carbon dioxide, 88.18 kg/s. However, other scenarios including 3, 4, 5, 7, 8, and 9 are equal in CO_2 production comparison.

8. Conclusion

Distributed generation as a viable solution to the energy crisis has gained in popularity in recent years due to reduced transmission losses and improved efficiency. Hence, in this study, a cogeneration system is investigated in multiple scenarios to meet electricity and heating demand or electricity and cooling need, simultaneously. The cogeneration system is initially modeled in the EES software. Then, the proposed system is studied in multiple scenarios.

The proposed gas turbine operates with a flow rate of 0.18848 kg/s and with a specific composition. The flow rate of input air to the compressor is optimized and is equal to 0.080316 kg/s. Moreover, the turbine has an efficiency of 34% and the UFR of 16536.6 kJ/kg. On the condition that waste heat of the flue gas discharged from the turbine, is not recovered, a large amount of energy may be lost. Comparing the obtained results of the designed scenarios, the following conclusion can be drawn:

(1) A proper configuration of the energy system can provide electricity, heating and cooling need with lower energy consumption.
(2) The optimum system can be selected based on the UFR for simultaneous electricity and heating generation or electricity and cooling generation. Thus, scenario No. 5 with the UFR of 45325.50 kJ/kg has the most efficient performance among the scenarios considering to meet electricity and cooling demand. Scenario No. 1 has the lowest UFR with a value of 21741.70 kJ/kg which is insufficient for energy production. Moreover, to produce electricity and heating, scenario No. 7 has the optimum performance with the UFR value of 39541.90 kJ/kg. However, scenario No. 6 with the UFR of 24425.98 kJ/kg is also inefficient.
(3) For combined heating and power generation, reduction of pressure in the recovery system of the gas turbine causes output temperature of the heat exchanger to decrease which significantly affects the UFR value.
(4) The most optimum system for electricity and cooling generation consists of SEAC, DEAC and gas turbine.

Declaration of Competing Interest

The authors declare that they have no known competing financial interests or personal relationships that could have appeared to influence the work reported in this paper.

References

[1] Fuel shares of total primary energy supply n.d. https://www.iea.org/publications/freepublications/publication/key-world-energy-statistics-%0A2015.html.

[2] Safari F, Tavasoli A, Ataei A. Gasification of sugarcane bagasse in supercritical water media for combined hydrogen and power production: a novel approach. Int J Environ Sci Technol 2016;13:2393–400. https://doi.org/10.1007/s13762-016-1055-7.

[3] Naeimi A, Bidi M, Ahmadi MH, Kumar R, Sadeghzadeh M, Alhuyi Nazari M. Design and exergy analysis of waste heat recovery system and gas engine for power generation in Tehran cement factory. Therm Sci Eng Prog 2019;9:299–307. https://doi.org/10.1016/j.tsep.2018.12.007.

[4] Wu Q, Ren H, Gao W, Ren J. Modeling and optimization of distributed energy supply network with power and hot water interchanges. Appl Therm Eng 2016;94:635–43. https://doi.org/10.1016/J.APPLTHERMALENG.2015.10.157.

[5] Martínez-Lera S, Ballester J. A novel method for the design of CHCP (combined heat, cooling and power) systems for buildings. Energy 2010;35:2972–84. https://doi.org/10.1016/J.ENERGY.2010.03.032.

[6] Ahmadi MH, Alhuyi Nazari M, Sadeghzadeh M, Pourfayaz F, Ghazvini M, Ming T, et al. Thermodynamic and economic analysis of performance evaluation of all the thermal power plants: a review. Energy Sci Eng 2019;7:30–65. https://doi.org/10.1002/ese3.223.

[7] Sanaye S, Ghafurian MM, Dastjerd FT. Applying relative net present or relative net future worth benefit and exergy efficiency for optimum selection of a natural gas engine based cchp system for a hotel building. J Nat Gas Sci Eng 2016;34:305–17. https://doi.org/10.1016/J.JNGSE.2016.06.038.

[8] Mohammadi A, Ashouri M, Ahmadi MH, Bidi M, Sadeghzadeh M, Ming T. Thermoeconomic analysis and multiobjective optimization of a combined gas turbine, steam, and organic Rankine cycle. Energy Sci Eng 2018;6:506–22. https://doi.org/10.1002/ese3.227.

[9] Shams Ghoreishi SM, Akbari Vakilabadi M, Bidi M, Khoeini Poorfar A, Sadeghzadeh M, Ahmadi MH, et al. Analysis, economical and technical enhancement of an organic Rankine cycle recovering waste heat from an exhaust gas stream. Energy Sci Eng 2019:1–25. https://doi.org/10.1002/ese3.274.

[10] Gu Q, Ren H, Gao W, Ren J. Integrated assessment of combined cooling heating and power systems under different design and management options for residential buildings in Shanghai. Energy Build 2012;51:143–52. https://doi.org/10.1016/J.ENBUILD.2012.04.023.

[11] Mostafavi Tehrani SS, Saffar-Avval M, Mansoori Z, Behboodi Kalhori S, Abbassi A, Dabir B, et al. Development of a CHP/DH system for the new town of Parand: an opportunity to mitigate global warming in Middle East. Appl Therm Eng 2013;59:298–308. https://doi.org/10.1016/J.APPLTHERMALENG.2013.05.016.

[12] Arsalis A, Alexandrou A. Thermoeconomic modeling and exergy analysis of a decentralized liquefied natural gas-fueled combined-cooling–heating-and-power plant. J Nat Gas Sci Eng 2014;21:209–20. https://doi.org/10.1016/J.JNGSE.2014.08.009.

[13] Liu M, Shi Y, Fang F. Combined cooling, heating and power systems: a survey. Renew Sustain Energy Rev 2014;35:1–22. https://doi.org/10.1016/J.RSER.2014.03.054.

[14] Chen X, Gong G, Wan Z, Zhang C, Tu Z. Performance study of a dual power source residential CCHP system based on PEMFC and PTSC. Energy Convers Manage 2016;119:163–76. https://doi.org/10.1016/J.ENCONMAN.2016.04.054.

[15] Ebrahimi M, Keshavarz A, Ebrahimi M, Keshavarz A. CCHP technology. Comb Cool Heat Power 2015:35–91. https://doi.org/10.1016/B978-0-08-099985-2.00002-0.

[16] Zheng CY, Wu JY, Zhai XQ, Wang RZ. Impacts of feed-in tariff policies on design and performance of CCHP system in different climate zones. Appl Energy 2016;175:168–79. https://doi.org/10.1016/J.APENERGY.2016.05.005.

[17] Li B, Hu P, Zhu N, Lei F, Xing L. Performance analysis and optimization of a CCHP-GSHP coupling system based on quantum genetic algorithm. Sustain Cities Soc 2019;46:101408. https://doi.org/10.1016/J.SCS.2018.12.036.

[18] Pagliarini G, Corradi C, Rainieri S. Hospital CHCP system optimization assisted by TRNSYS building energy simulation tool. Appl Therm Eng 2012;44:150–8. https://doi.org/10.1016/J.APPLTHERMALENG.2012.04.001.

[19] Jabbari B, Tahouni N, Ataei A, Panjeshahi MH. Design and optimization of CCHP system incorporated into kraft process, using Pinch Analysis with pressure drop consideration. Appl Therm Eng 2013;61:88–97. https://doi.org/10.1016/J.APPLTHERMALENG.2013.01.050.

[20] Zhou Z, Liu P, Li Z, Pistikopoulos EN, Georgiadis MC. Impacts of equipment off-design characteristics on the optimal design and operation of combined cooling, heating and power systems. Comput Chem Eng 2013;48:40–7. https://doi.org/10.1016/J.COMPCHEMENG.2012.08.007.

[21] Wang JL, Wu JY, Zheng CY. Simulation and evaluation of a CCHP system with exhaust gas deep-recovery and thermoelectric generator. Energy Convers Manage

2014;86:992–1000. https://doi.org/10.1016/J.ENCONMAN.2014.06.036.

[22] Al-Qattan A, ElSherbini A, Al-Ajmi K. Solid oxide fuel cell application in district cooling. J Power Sources 2014;257:21–6. https://doi.org/10.1016/J.JPOWSOUR. 2014.01.099.

[23] Jayasekara S, Halgamuge SK. A combined effect absorption chiller for enhanced performance of combined cooling heating and power systems. Appl Energy 2014;127:239–48. https://doi.org/10.1016/J.APENERGY.2014.04.035.

[24] Ebrahimi M, Keshavarz A. Designing an optimal solar collector (orientation, type and size) for a hybrid-CCHP system in different climates. Energy Build 2015;108:10–22. https://doi.org/10.1016/J.ENBUILD.2015.08.056.

[25] Hanafizadeh P, Eshraghi J, Ahmadi P, Sattari A. Evaluation and Sizing of a CCHP System for a Commercial and Office Buildings. J Build Eng 2016;5:67–78. https:// doi.org/10.1016/j.jobe.2015.11.003.

[26] Li Y, Hu R. Exergy-analysis based comparative study of absorption refrigeration and electric compression refrigeration in CCHP systems. Appl Therm Eng 2016;93:1228–37. https://doi.org/10.1016/J.APPLTHERMALENG.2015.10.079.

[27] Gang W, Wang S, Xiao F, Gao D. Performance Assessment of District Cooling System Coupled with Different Energy Technologies in Subtropical Area. Energy Procedia 2015;75:1235–41. https://doi.org/10.1016/J.EGYPRO.2015.07.166.

[28] Wang J, Wu J, Wang H. Experimental investigation of a dual-source powered absorption chiller based on gas engine waste heat and solar thermal energy. Energy 2015;88:680–9. https://doi.org/10.1016/J.ENERGY.2015.05.103.

[29] Chaiyat N, Kiatsiriroat T. Analysis of combined cooling heating and power generation from organic Rankine cycle and absorption system. Energy 2015;91:363–70. https://doi.org/10.1016/J.ENERGY.2015.08.057.

[30] Goyal R, Sharma D, Soni SL, Gupta PK, Johar D, Sonar D. Performance and emission analysis of CI engine operated micro-trigeneration system for power, heating and space cooling. Appl Therm Eng 2015;75:817–25. https://doi.org/10.1016/J. APPLTHERMALENG.2014.10.026.

[31] Wang J, Mao T, Sui J, Jin H. Modeling and performance analysis of CCHP (combined cooling, heating and power) system based on co-firing of natural gas and biomass gasification gas. Energy 2015;93:801–15. https://doi.org/10.1016/J. ENERGY.2015.09.091.

[32] Wang Z, Han W, Zhang N, Liu M, Jin H. Proposal and assessment of a new CCHP system integrating gas turbine and heat-driven cooling/power cogeneration. Energy Convers Manage 2017;144:1–9. https://doi.org/10.1016/J.ENCONMAN.2017.04. 043.

[33] Han B-C, Cheng W-L, Li Y-Y, Nian Y-L. Thermodynamic analysis of heat driven Combined Cooling Heating and Power system (CCHP) with energy storage for long distance transmission. Energy Convers Manage 2017;154:102–17. https://doi.org/ 10.1016/J.ENCONMAN.2017.10.058.

[34] Caliano M, Bianco N, Graditi G, Mongibello L. Design optimization and sensitivity analysis of a biomass-fired combined cooling, heating and power system with thermal energy storage systems. Energy Convers Manage 2017;149:631–45. https://doi.org/10.1016/J.ENCONMAN.2017.07.048.

[35] Wang J, Lu Z, Li M, Lior N, Li W. Energy, exergy, exergoeconomic and environmental (4E) analysis of a distributed generation solar-assisted CCHP (combined cooling, heating and power) gas turbine system. Energy 2019;175:1246–58. https://doi.org/10.1016/J.ENERGY.2019.03.147.

[36] Mehrpooya M, Sadeghzadeh M, Rahimi A, Pouriman M. Technical performance analysis of a combined cooling heating and power (CCHP) system based on solid oxide fuel cell (SOFC) technology – A building application. Energy Convers Manage 2019;198:111767 https://doi.org/10.1016/J.ENCONMAN.2019.06.078.

[37] Sheykhi M, Chahartaghi M, Balakheli MM, Hashemian SM, Miri SM, Rafiee N. Performance investigation of a combined heat and power system with internal and external combustion engines. Energy Convers Manage 2019;185:291–303. https:// doi.org/10.1016/J.ENCONMAN.2019.01.116.

[38] Wu D, Han Z, Liu Z, Zhang H. Study on configuration optimization and economic feasibility analysis for combined cooling, heating and power system. Energy Convers Manage 2019;190:91–104. https://doi.org/10.1016/J.ENCONMAN.2019. 04.004.

[39] Abbasi M, Chahartaghi M, Hashemian SM. Energy, exergy, and economic evaluations of a CCHP system by using the internal combustion engines and gas turbine as prime movers. Energy Convers Manage 2018;173:359–74. https://doi.org/10. 1016/J.ENCONMAN.2018.07.095.

[40] Adhami H, Khalilarya S, Jafarmadar S, Ebrahimi M. Thermodynamic feasibility study of a suggested portable personal micro trigeneration system based on micro-gas turbine and micro-absorption chiller. Appl Therm Eng 2018;144:45–58. https:// doi.org/10.1016/J.APPLTHERMALENG.2018.08.018.

[41] Wang X, Yang C, Huang M, Ma X. Multi-objective optimization of a gas turbine-based CCHP combined with solar and compressed air energy storage system. Energy Convers Manage 2018;164:93–101. https://doi.org/10.1016/J.ENCONMAN.2018. 02.081.

[42] Chen LG, Tao GS, Sun FR. Finite-time exergoeconomic optimal performance for an irreversible gas turbine closed-cycle cogeneration plant. Int J Sustain Energy 2012;31:43–58. https://doi.org/10.1080/1478646X.2010.534795.

[43] Tao GS, Chen LG, Sun FR, Wu C. Exergoeconomic performance optimisation for an endoreversible simple gas turbine cycle cogeneration plant. Int J Ambient Energy 2009;30:115–24. https://doi.org/10.1080/01430750.2009.9675797.

[44] Chen LG, Yang B, Ding ZM, Liu XW, Meng FK. Performance investigation of an open simple-cycle gas turbine CCHP plant driven by basic oxygen furnace gas in China's steelmaking plants. ECOS 2018, 31st Int. Conf. Effic. Cost, Optim. Simul. Environ. Impact Energy Syst., Guimaraes, Portugal: 2018, p. paper No. 98.

[45] Tao GS, Chen LG, Sun FR. Exergoeconomic performance optimization for an endoreversible regenerative gas turbine closed-cycle cogeneration plant. Rev Mex Física 2009;55:192–200.

[46] Chen L G, Yang B, Feng H J, Ding Z M. Modelling, analyses and optimization for exergy performance an irreversible intercooled regenerated Brayton CHP plant. Part 1. Thermodynamic modeling and parametric analyses. ASME International Mechanical Engineering Congress & Exposition (IMECE) Conference, Tampa, Florida, November 3-9, 2017, IMECE2017-70045. doi: 10.1115/IMECE2017-70045.

[47] Yang B, Chen L G, Feng H J, Ding Z M. Modelling, analyses and optimization for exergy performance an irreversible intercooled regenerated Brayton CHP plant. Part 2. Performance optimization. ASME International Mechanical Engineering Congress & Exposition (IMECE) Conference, Tampa, Florida, November 3–9, 2017, IMECE2017-70046. doi: 10.1115/IMECE2017-70046.

[48] Chen LG, Feng HJ, Sun FR. Exergoeconomic performance optimization for a combined cooling, heating and power generation plant with an endoreversible closed Brayton cycle. Math Comput Model 2011;54:2785–801. https://doi.org/10.1016/J. MCM.2011.06.067.

[49] Feng HJ, Chen LG, Sun FR. Exergoeconomic optimal performance of an irreversible closed Brayton cycle combined cooling, heating and power plant. Appl Math Model 2011;35:4661–73. https://doi.org/10.1016/J.APM.2011.03.036.

[50] Chen LG, Feng HJ, Sun FR. Exergy optimisation of irreversible closed Brayton cycle combined cooling, heating and power plant. J Energy Inst 2013;86:97–106. https:// doi.org/10.1179/1743967112Z.00000000048.

[51] Yang B, Chen LG, Ge YL, Sun FR. Exergy analyses of an endoreversible closed regenerative Brayton cycle CCHP plant. Int J Energy Environ Econ 2014;5:655–68.

[52] Feng HJ, Chen LG, Xie ZH, Ge YL. Maximum exergy output rate for an endoreversible closed Brayton cycle combined cooling, heating and power plant. 2017 American Society of Thermal and Fluids Engineers (ASTFE) Conference and 4th International Workshop on Heat Transfer (IWHT), April 2-5, 2017, Las Vegas, NV. Paper ID: TFEC-IWHT2017-18311. doi:10.1615/TFEC2017.fna.018311.

[53] Andresen B, Berry RS, Ondrechen MJ, Salamon P. Thermodynamics for processes in finite time. ACC Chem Res 1984;17:266–71. https://doi.org/10.1021/ ar00104a001.

[54] Bejan A. Entropy generation minimization: the new thermodynamics of finite-size devices and finite-time processes. J Appl Phys 1996;79:1191–218. https://doi.org/ 10.1063/1.362674.

[55] Chen LG, Feng HJ, Xie ZH. Generalized thermodynamic optimization for iron and steel production processes: theoretical exploration and application cases. Entropy 2016;18(10):353. https://doi.org/10.3390/e18100353.

[56] Badescu V. Optimal control in thermal engineering. New York: Springer; 2017.

[57] Kaushik SC, Tyagi SK, Kumar P. Finite time thermodynamics of power and refrigeration cycles. New York: Springer; 2018.

[58] Torres-Reyes E, Cervantes-de Gortari J, Ibarra-Salazar B, Picon-Nuñez M. A design method of flat-plate solar collectors based on minimum entropy generation. Exergy. An Int J 2001;1:46–52. https://doi.org/10.1016/S1164-0235(01)00009-7.

[59] Chen LG, Wu C, Sun FR. Finite time thermodynamic optimization or entropy generation minimization of energy systems. J Non-Equilib Thermodyn 1999;24(4):327–59. https://doi.org/10.1515/JNETDY.1999.020.

[60] Wu C, Chen LG, Chen JC. Recent advances in finite time thermodynamics. New York: Nova Science Publishers; 1999.

[61] Durmayaz A, Sogut OS, Sahin B, Yavuz H. Optimization of thermal systems based on finite-time thermodynamics and thermoeconomics. Prog Energy Combust Sci 2004;30:175–217. https://doi.org/10.1016/J.PECS.2003.10.003.

[62] Chen LG, Sun FR. Advances in finite time thermodynamics: analysis and optimization. New York: Nova Science Publishers; 2004.

[63] Andresen B. Current trends in finite-time thermodynamics. Angew Chemie Int Ed 2011;50:2690–704. https://doi.org/10.1002/anie.201001411.

[64] Ge YL, Chen LG, Sun FR. Progress in finite time thermodynamic studies for internal combustion engine cycles. Entropy 2016;18(4):139. https://doi.org/10.3390/ e18040139.

[65] Sieniutycz S. Thermodynamic approaches in engineering systems. Oxford: Elsevier; 2016.

[66] Chen LG, Xia SJ, Sun FR. Entropy generation minimization for isothermal crystallization processes with a generalized mass diffusion law. Int J Heat Mass Transf 2018;116:1–8.

[67] Ge YL, Chen LG, Qin XY. Effect of specific heat variations on irreversible Otto cycle performance. Int J Heat Mass Transf 2018;122:403–9.

[68] Wu ZX, Chen LG, Ge YL, Sun FR. Thermodynamic optimization for an air-standard irreversible Dual-Miller cycle with linearly variable specific heat ratio of working fluid. Int J Heat Mass Transf 2018;124:46–57.

[69] Chen LG, Wang C, Xia SJ, Sun FR. Thermodynamic analysis and optimization of extraction process of CO2 from acid seawater by using hollow fiber membrane contactor. Int J Heat Mass Transf 2018;124:1310–20.

[70] Chen LG, Zhang L, Xia SJ, Sun FR. Entropy generation minimization for hydrogenation of CO2 to light olefins. Energy 2018;147:187–96.

[71] Shen JF, Chen LG, Ge YL, Zhu FL, Wu ZX. Optimum ecological performance of irreversible reciprocating Maisotsenko-Brayton cycle. The Euro. Phys. J. Plus 2019;134(6):293.

[72] Qiu SS, Ding ZM, Chen LG, Meng FK, Sun FR. Optimal performance regions of energy selective electron cooling devices consisting of three reservoirs. Euro Phys J Plus 2019;134(6):273.

[73] Chen LG, Ge YL, Qin XY, Xie ZH. Exergy-based ecological optimization for a four-temperature-level absorption heat pump with heat resistance, heat leakage and internal irreversibility. Int J Heat Mass Transf 2019;129:855–61.

[74] Zhang L, Xia SJ, Chen LG, Wang C, Feng HJ. Entropy generation rate minimization for hydrocarbon synthesis reactor from carbon dioxide and hydrogen. Int J Heat Mass Transf 2019;137:1112–23.

[75] Li PL, Chen LG, Xia SJ, Zhang L. Entropy generation rate minimization for in

methanol synthesis via CO_2 hydrogenation reactor. Entropy 2019;21(2):174.

[76] Ding ZM, Chen LG, Ge YL, Xie ZH. Optimal performance regions of an irreversible energy selective electron heat engine with double resonance. Sci China Tech Sci 2019;62(3):337–405.

[77] Liu XW, Chen LG, Wei SH. Meng F K. Optimal ecological performance investigation of a quantum harmonic oscillator Brayton refrigerator. Trans ASME J Therm Sci Eng Appl 2020,;12(1):011007.

[78] Moghimi M, Emadi M, Ahmadi P, Moghadasi H. 4E analysis and multi-objective optimization of a CCHP cycle based on gas turbine and ejector refrigeration. Appl Therm Eng 2018;141:516–30. https://doi.org/10.1016/J.APPLTHERMALENG. 2018.05.075.

[79] Noroozian A, Mohammadi A, Bidi M, Ahmadi MH. Energy, exergy and economic analyses of a novel system to recover waste heat and water in steam power plants. Energy Convers Manage 2017;144:351–60. https://doi.org/10.1016/J. ENCONMAN.2017.04.067.

[80] Mohammadi A, Bidi M, Ahmadi MH. Economic evaluation of different scenarios for gas turbine waste heat recovery to produce water and power. Int J Ambient Energy 2017;38:727–34. https://doi.org/10.1080/01430750.2016.1195776.

[81] Hou S, Zhang F, Yu L, Cao S, Zhou Y, Wu Y, et al. Optimization of a combined cooling, heating and power system using CO2 as main working fluid driven by gas turbine waste heat. Energy Convers Manage 2018;178:235–49. https://doi.org/10. 1016/J.ENCONMAN.2018.09.072.

[82] Cengel YA, Boles MA. Thermodyamics: an engineering approach. McGraw- Hill Education; 2015. doi: 10.1017/CBO9781107415324.004.

[83] Mossi Idrissa AK, Goni Boulama K. Advanced exergy analysis of a combined Brayton/Brayton power cycle. Energy 2019;166:724–37. https://doi.org/10.1016/ J.ENERGY.2018.10.117.

[84] Bou Nader WS, Mansour CJ, Nemer MG. Optimization of a Brayton external combustion gas-turbine system for extended range electric vehicles. Energy 2018;150:745–58. https://doi.org/10.1016/J.ENERGY.2018.03.008.